



Turing pattern dynamics and adaptive discretization for a super-diffusive Lotka-Volterra model

Mostafa Bendahmane¹ · Ricardo Ruiz-Baier² ·
Canrong Tian³

Received: 25 July 2014 / Revised: 9 June 2015 / Published online: 29 July 2015
© Springer-Verlag Berlin Heidelberg 2015

Abstract In this paper we analyze the effects of introducing the fractional-in-space operator into a Lotka-Volterra competitive model describing population super-diffusion. First, we study how cross super-diffusion influences the formation of spatial patterns: a linear stability analysis is carried out, showing that cross super-diffusion triggers Turing instabilities, whereas classical (self) super-diffusion does not. In addition we perform a weakly nonlinear analysis yielding a system of amplitude equations, whose study shows the stability of Turing steady states. A second goal of this contribution is to propose a fully adaptive multiresolution finite volume method that employs shifted Grünwald gradient approximations, and which is tailored for a larger class of systems involving fractional diffusion operators. The scheme is aimed at efficient dynamic mesh adaptation and substantial savings in computational burden. A numerical simulation of the model was performed near the instability boundaries, confirming the behavior predicted by our analysis.

✉ Canrong Tian
tiancanrong@163.com

Mostafa Bendahmane
mostafa.bendahmane@u-bordeaux2.fr

Ricardo Ruiz-Baier
ricardo.ruizbaier@unil.ch

¹ Institut de Mathématiques de Bordeaux, Université Victor, Segalen Bordeaux 2,
33076 Bordeaux Cedex, France

² Institute of Earth Sciences, University of Lausanne,
1015 Lausanne, Switzerland

³ Department of Basic Sciences, Yancheng Institute of Technology,
Yancheng 224003, China

Keywords Turing instability · Pattern formation · Amplitude equations · Super-diffusion · Cross-diffusion · Linear stability · Lévy flights · Finite volume approximation · Fully adaptive multiresolution

Mathematics Subject Classification Primary 35B35; Secondary 35B40 · 47D20

1 Introduction and formulation of the model

In population dynamics, a spatially homogeneous competitive system can be modelled with the so-called Lotka-Volterra system of differential equations written in the form

$$\begin{aligned}\frac{du}{dt} &= u(a_1 - b_{11}u - b_{12}v), \\ \frac{dv}{dt} &= v(a_2 - b_{21}u - b_{22}v).\end{aligned}$$

In this model, u and v represent the population densities of two competitors, a_i are the birth (or generation) rates of the i -th population, the coefficients b_{ii} measure the intra-population competitive effect of the two competitors, $i = 1, 2$, and b_{12}, b_{21} stand for a factor representing the inter-population competitive effects of u on v , and of v on u , respectively.

As usual, the system variables are rescaled, giving

$$\bar{u} = \frac{b_{11}}{a_1}u, \quad \bar{v} = \frac{b_{22}}{a_1}v, \quad \bar{t} = a_1 t, \quad a = \frac{a_2}{a_1}, \quad b = \frac{b_{21}}{b_{11}}, \quad c = \frac{b_{12}}{b_{22}},$$

and after dropping the bars, we find that the interaction of u and v is governed by the following system of ordinary differential equations

$$\frac{du}{dt} = u(1 - u - cv), \quad \frac{dv}{dt} = v(a - bu - v).$$

The population densities within a spatially heterogeneous environment imply the introduction of normal diffusive terms into the evolution system (see e.g. [Okubo and Levin 2002](#)). At molecular level, classical diffusion arises as the result of standard Brownian motion, and it is typically characterized by the dependence of the mean square displacement of a randomly walking particle on time $\langle(\Delta x)^2\rangle \sim t$. Apart from classical (or normal) diffusion, molecules may undergo *anomalous* diffusion effects (as discussed in e.g. [Bouchard and Georges 1990](#); [Metzler and Klafter 2000, 2004](#); [Sokolov et al. 2002](#); [Golovin et al. 2008](#); [Gambino et al. 2013](#)). These phenomena (in contrast to normal diffusion) are rather characterized by the more general dependence

$$\langle(\Delta x)^2\rangle = 2dK_\alpha t^\alpha,$$

where d is the (embedding) spatial dimension, K_α is a generalized diffusion constant, and the exponent α is not necessarily an integer. For $\alpha = 1$, anomalous diffusion

reduces to normal diffusion, with the classical diffusion coefficient set to K_1 . For $\alpha < 1$ ($\alpha > 1$), the diffusion process is slower (faster) than normal diffusion, in which case it is called sub-diffusive (resp., super-diffusive). An important limiting case of super-diffusion corresponds to Lévy flights (Metzler and Klafter 2004), which is a phenomenon occurring in systems where there are long jumps of particles, i.e., with a jump size distribution having infinite moments. In the context of population dynamics, super-diffusion (rather than classical diffusion) has been employed as a more appropriate way to describe the motion of animals under certain circumstances (Viswanathan et al. 1996; Schmitt and Seuront 2001; Toner et al. 2005).

In this context, the present model is motivated by recent studies showing that the front dynamics of the complex movement of populations (humans or animals), may be driven by fractional Lévy flights (c.f. Buchanan 2008). Notice that Lévy flights are super-diffusive, that is, they represent faster dispersion than purely Gaussian random-walk. Patterns associated to Lévy flights have been observed in the movement of different species ranging from albatrosses (Viswanathan et al. 1996), marine predators (Sims et al. 2008), monkeys (Ramos-Fernandez et al. 2004), or mussels (Jager et al. 2011). In addition, some recent studies suggest that modern diseases (such as SARS or avian influenza) cannot be represented by the classical reaction-diffusion systems (where a Gaussian dispersion process is typically assumed). These models are only applicable when each class of the population (e.g. the infective and susceptible) travels short distances as compared to geographical scales. The aforementioned diseases can spread around the world quickly (in a few weeks) and seem to follow Lévy-flight mobility patterns (for an application, see Hufnagel et al. 2004).

Here the population density is assumed to solve a fractional-order diffusion equation. We also refer to Brockmann et al. (2006), where the authors show that the density of bank notes originating from a given city is a solution of a particular fractional equation. They suggest that an epidemic spread could be modelled employing a similar equation. Moreover, Brockmann (2009) proposes a SIR model that includes a fractional diffusion.

To take into account the movement of populations with Lévy flight type, we are led to the following fractional reaction diffusion system:

$$\begin{aligned}\partial_t u &= d_{11} \nabla^\gamma u + d_{12} \nabla^\gamma v + u(1 - u - cv), \\ \partial_t v &= d_{22} \nabla^\gamma v + v(a - bu - v).\end{aligned}\tag{1.1}$$

Here d_{11} and d_{22} are the self super-diffusive coefficients, and d_{12} is the cross super-diffusive coefficient. The so-called Weyl fractional operator ∇^γ ($1 < \gamma \leq 2$) represents the super-diffusion, whose Fourier transform is $\widehat{\nabla^\gamma u}(\mathbf{k}) = -|\mathbf{k}|^\gamma \hat{u}(\mathbf{k})$. In one dimension, the Weyl operator is equivalent to the Riesz operator

$$\begin{aligned}\nabla^\gamma u &= -\frac{1}{2 \cos(\pi \gamma / 2)} (D_+^\gamma u + D_-^\gamma u), \\ D_+^\gamma u &= \frac{1}{\Gamma(2 - \gamma)} \frac{d^2}{dx^2} \int_{-\infty}^x \frac{u(\xi, t)}{(x - \xi)^{\gamma - 1}} d\xi,\end{aligned}$$

$$D_-^\gamma u = \frac{1}{\Gamma(2-\gamma)} \frac{d^2}{dx^2} \int_x^\infty \frac{u(\xi, t)}{(\xi - x)^{\gamma-1}} d\xi,$$

where $\Gamma(\cdot)$ stands for the Gamma function. In higher dimensions, the Weyl operator can be represented by the fractional Laplacian operator $\nabla^\gamma = -(-\Delta)^{\gamma/2}$, and consequently system (1.1) can be written as

$$\begin{aligned} \partial_t u + d_{11}(-\Delta)^{\gamma/2} u + d_{12}(-\Delta)^{\gamma/2} v &= u(1 - u - cv), \\ \partial_t v + d_{22}(-\Delta)^{\gamma/2} v &= v(a - bu - v). \end{aligned} \quad (1.2)$$

In our model (1.2), the spatial dynamics are represented by a nonlocal differential operator denoted $(-\Delta)^\alpha$ with $\alpha = 2/\gamma$. We recall that Lévy flights spread proportionally to time as $t^{1/\gamma}$, whereas Gaussian motion spreads proportional to time in the form $t^{1/2}$. Hence the mean square displacement undergoing Lévy flights would grow faster than Gaussian motion, at a rate of $t^{2/\gamma}$. It is also noted that Lévy flights do not possess a finite mean squared displacement, whose physical significance is questioned as particles with a finite mass should not execute long jumps instantaneously. However, in some cases such as those outlined above, their description in terms of Lévy flights do correspond to physically-based principles (see also Metzler and Klafter 2000).

Recall that in classical reaction-diffusion systems the density of populations follows a Gaussian diffusive process (the distribution of random displacements has a finite variance), as a consequence of the Central Limit Theorem. In our study, we actually assume that the displacement of populations does not necessarily have a finite variance and so the standard version of the mentioned theorem cannot be applied. In this case the density of populations tends towards a stable Lévy flight with exponent α (see Metzler and Klafter 2000; Hanert et al. 2011 for more details). Based on e.g. thermodynamic considerations, it is possible to assume dependence of the model coefficients (and in particular, the cross-diffusion term) on the concentration of u . After performing the Taylor expansion of the physical cross-diffusion around the positive equilibrium, we end up with the cross-diffusive term $d_{12}\nabla^\gamma v$ as a linear term. In this context, since our main objective is to consider the dynamical behavior of the system around the stationary state, we postulate that looking only at the linear cross-diffusion $d_{12}\nabla^\gamma v$ in Eq. (1.1) will suffice.

Pattern formation in reaction diffusion systems with anomalous diffusion has recently received considerable attention (Gafiychuk and Datsko 2006; Henry et al. 2005; Henry and Wearne 2002; Langlands et al. 2007; Weiss 2003; Golovin et al. 2008; Gambino et al. 2013). For instance, it was shown that sub-diffusion suppresses the formation of Turing patterns (Weiss 2003). In Yadav and Horsthemke (2006), Yadav et al. (2008), Nec and Nepomnyashchy (2007) and Nec and Nepomnyashchy (2008) the authors consider sub-diffusive reaction-diffusion systems and rigorously derive the conditions for Turing instabilities. It was also found in one dimensional systems that anomalous heat conduction can happen as a consequence of the anomalous diffusion (Li and Wang 2003). Additionally, in systems with Lévy flights, the emergence of spiral waves and chemical turbulence from the nonlinear dynamics of oscillating reaction diffusion patterns was investigated in Nec et al. (2008). The authors

in Golovin et al. (2008) explored the effects of super-diffusion on pattern formation and pattern selection in the substrate-depleted Brusselator model, and found that Turing instability can occur even when diffusion of the inhibitor is slower than that of the activator. However, results on the nonlinear dynamics and Turing pattern selection in reaction diffusion systems with cross super-diffusion remain limited.

The effect of pattern formation of the Lotka–Volterra competitive model with normal diffusion and cross diffusion has been extensively investigated (see Horstmann 2007; Jüngel 2010 for some reviews). In Lou and Ni (1996) and Lou et al. (2001), the authors show that the Lotka–Volterra competitive system only with normal diffusion does not meet the conditions for a Turing instability to occur, whereas cross-diffusion drives the onset of Turing instability. In contrast, here we consider the effect of cross Lévy flights and super-diffusion on Turing patterns, and focus on the mode of pattern formation and the stability of the emerging patterns.

The remainder of this paper has been structured in the following way. In Sect. 2 we develop a linear stability analysis of the steady state of the system, which in turn provide the Turing parameter space that identifies regions where Turing bifurcations are expected. Section 3 is devoted to the derivation of a set of coupled amplitude equations, obtained by a weakly nonlinear analysis. Next, an analysis of these equations yields sufficient conditions to ensure so-called super-critical bifurcations. We also show how the stability of the Turing steady states is affected by these conditions. A fully adaptive finite volume – multiresolution method for the space-time discretization of (1.2) is proposed and discussed in Sect. 4. A simple numerical example is performed to confirm the results of the analysis. The weak solvability analysis of system (1.2) is also analyzed, and condensed in the appendix of the manuscript. We use the well-known Faedo–Galerkin strategy and the Kruzhkov compactness result to establish the existence of weak solutions. Our paper closes with a brief discussion in Sect. 5.

2 Linear stability analysis

In this section, we provide essential conditions to drive the Turing bifurcation by analyzing the linear stability of the uniform equilibrium state of (1.1). Notice that system (1.1) has a unique positive equilibrium $(u^*, v^*) = (\frac{1-ac}{1-bc}, \frac{a-b}{1-bc})$ if and only if

$$b < a < \frac{1}{c}. \quad (2.1)$$

Moreover, one can readily verify that (2.1) ensures that the positive equilibrium (u^*, v^*) is stable under any spatially homogeneous perturbation.

In order to carry out the linear stability analysis of (1.1), we set $\bar{u} = u - u^*$, $\bar{v} = v - v^*$, and substitute them in the system (1.1). By dropping the bars, we write the Taylor expansion form of the system (1.1) at the positive equilibrium as follows:

$$\begin{aligned} \partial_t u &= d_{11} \nabla^\gamma u + d_{12} \nabla^\gamma v - u^* u - c u^* v - u^2 - c u v, \\ \partial_t v &= d_{22} \nabla^\gamma v - b v^* u - v^* v - b u v - v^2. \end{aligned} \quad (2.2)$$

Let us further assume that the perturbation of (1.1) is periodic with respect to time. Hence the conditions of the classical Fourier theorem are met, and we seek the general solution

$$\begin{pmatrix} u \\ v \end{pmatrix} = \begin{pmatrix} c_1 \\ c_2 \end{pmatrix} \exp(\sigma t + i\mathbf{k} \cdot \mathbf{x}) \quad (2.3)$$

to the linearization of the problem (2.2) as a superposition of normal modes. Here σ is the growth rate of the perturbation in time t , i denotes the imaginary unit, with $i^2 = -1$, and \mathbf{k} is its wave vector. Suggested by the definition of the Weyl fractional operator ∇^γ , we focus on the time integration in Fourier space. Substituting (2.3) into the linearization of Eq. (2.2), we obtain the following matrix equation

$$\begin{pmatrix} \sigma + u^* + d_{11}k^\gamma & cu^* + d_{12}k^\gamma \\ bv^* & \sigma + v^* + d_{22}k^\gamma \end{pmatrix} \begin{pmatrix} c_1 \\ c_2 \end{pmatrix} = \begin{pmatrix} 0 \\ 0 \end{pmatrix},$$

where the Euclidean norm $k = |\mathbf{k}|$ is the wavenumber of the perturbation. Therefore, we are left to the dispersion relation

$$\sigma^2 + g(k)\sigma + h(k) = 0,$$

where

$$\begin{aligned} g(k) &:= u^* + v^* + (d_{11} + d_{22})k^\gamma, \\ h(k) &:= d_{11}d_{22}k^{2\gamma} + (d_{11}v^* + d_{22}u^* - d_{12}bv^*)k^\gamma + (1 - bc)u^*v^*. \end{aligned}$$

We stress that the corresponding equilibrium can lose its stability via Turing bifurcation if and only if $h(k) \leq 0$. Moreover, note that in the absence of cross super-diffusion one has $h(k) > 0$, which implies that in this particular case, only the cross super-diffusion effect can induce Turing bifurcation. Notice that $h(k)$ has a single minimum (k_c, d_{12}^c) , which is attained whenever

$$\begin{aligned} d_{12}^c &= \frac{d_{11}v^* + d_{22}u^* + 2\sqrt{(1 - bc)d_{11}d_{22}u^*v^*}}{bv^*}, \\ k_c &= \left(\frac{\sqrt{(1 - bc)u^*v^*}}{\sqrt{d_{11}d_{22}}} \right)^{\frac{1}{\gamma}}. \end{aligned} \quad (2.4)$$

Summarizing, we have obtained a Turing instability threshold d_{12}^c , and we have identified the critical value of the wave number k_c . It is noticed that the behavior of the super-diffusive system is qualitatively the same as that of the system with normal diffusion. Relation (2.4) represents the bifurcations occurring in the parameter region spanned by the parameters a , c and d_{12} . These regimes are also depicted in Fig. 1. All Turing patterns are driven by parameters chosen in this region. In addition, Fig. 2 displays the real part of the eigenvalue corresponding to three different sets of parameters, as a function of the wavenumber, and we notice that the active wavenumber changes with the order of the fractional diffusion γ .

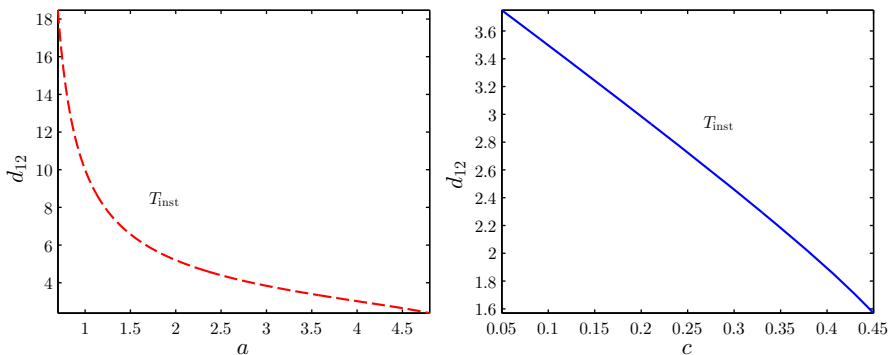
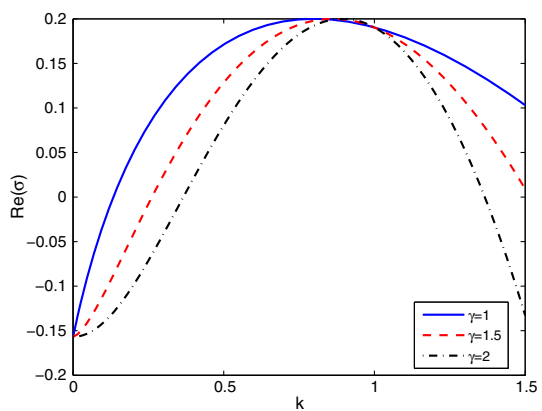


Fig. 1 Turing instability boundaries in the (a, d_{12}) and (c, d_{12}) planes. The instability region T_{inst} lies above the curves. The other parameters are $b = 1.5$, $d_{11} = 1$, $d_{22} = 1$

Fig. 2 Dispersion relation of the system (1.1) for three different $\gamma = 1, 1.5, 2$. The other parameters are $a = 2.5$, $b = 1.5$, $c = 0.2$, $d_{11} = 1$, $d_{22} = 1$, and $d_{12} = 1.8$



3 Diamond planform weakly nonlinear stability analysis

In order to study the dynamics of Turing patterns, we perform here a weakly nonlinear analysis of system (2.2) near the Turing instability threshold. In particular, we aim at analyzing the pattern selection mechanisms associated to diamonds and stripes. Let us consider system (2.2) defined in the whole two-dimensional space \mathbf{R}^2 . Weakly nonlinear analyses are typically based on the fact that Turing bifurcations are able to destabilize the homogeneous equilibrium, but only in case of perturbations with wave numbers close to the critical value k_c . In regimes near to the Turing onset $d_{12} = d_{12}^c$, the solutions can be described by a system of three active resonant pairs of modes $(\mathbf{k}_j, -\mathbf{k}_j)$, for $j = 1, 2, 3$. Each pair of modes form angles of $2\pi/3$ and $|\mathbf{k}_j| = k_c$. This fact implies that solutions of system (2.2) can be expanded as

$$\begin{pmatrix} u \\ v \end{pmatrix} = \sum_{j=1}^3 [A_j \exp(i\mathbf{k}_j \cdot x) + \bar{A}_j \exp(-i\mathbf{k}_j \cdot x)], \quad (3.1)$$

where \mathbf{A}_j and its conjugate $\bar{\mathbf{A}}_j$ stand, respectively, for the amplitudes associated with the modes \mathbf{k}_j and $-\mathbf{k}_j$, and $\mathbf{A}_j \equiv (A_j^u, A_j^v)^T$.

We introduce a scaled *slow* time variable $T = \varepsilon^2 t$, and expand both fields u and v , as well as the bifurcation parameter d_{12} , in the form

$$\begin{aligned} \begin{pmatrix} u \\ v \end{pmatrix} &= \varepsilon \begin{pmatrix} u_1 \\ v_1 \end{pmatrix} + \varepsilon^2 \begin{pmatrix} u_2 \\ v_2 \end{pmatrix} + \varepsilon^3 \begin{pmatrix} u_3 \\ v_3 \end{pmatrix} + \dots, \\ d_{12} - d_{12}^c &= \mu_2 \varepsilon^2 + O(\varepsilon^3). \end{aligned} \quad (3.2)$$

Since the amplitude \mathbf{A} is a variable that undergoes slow changes, it follows that

$$\partial_t \mathbf{A} = \varepsilon^2 \frac{\partial \mathbf{A}}{\partial T} + O(\varepsilon^3).$$

Substituting Eq. (3.2) into the system (2.2), we have

$$\begin{aligned} \varepsilon^3 \frac{\partial}{\partial T} \begin{pmatrix} u_1 \\ v_1 \end{pmatrix} &= \varepsilon \mathbf{L}_c \begin{pmatrix} u_1 \\ v_1 \end{pmatrix} + \varepsilon^2 \mathbf{L}_c \begin{pmatrix} u_2 \\ v_2 \end{pmatrix} + \varepsilon^3 \mathbf{L}_c \begin{pmatrix} u_3 \\ v_3 \end{pmatrix} - \varepsilon^3 \mu_2 k_c^\gamma \mathbf{M} \begin{pmatrix} u_1 \\ v_1 \end{pmatrix} \\ &\quad - \varepsilon^2 \begin{pmatrix} u_1^2 + cu_1 v_1 \\ bu_1 v_1 + v_1^2 \end{pmatrix} - \varepsilon^3 \begin{pmatrix} 2u_1 u_2 + cu_1 v_2 + cu_2 v_1 \\ bu_1 v_2 + bu_2 v_1 + 2v_1 v_2 \end{pmatrix}, \end{aligned}$$

where the involved matrices are defined as

$$\mathbf{L}_c = \begin{pmatrix} -u^* + d_{11} \nabla^\gamma & -cu^* + d_{12}^c \nabla^\gamma \\ -bv^* & -v^* + d_{22} \nabla^\gamma \end{pmatrix}, \quad \mathbf{M} = \begin{pmatrix} 0 & 1 \\ 0 & 0 \end{pmatrix}.$$

After collecting like powers of ε , we obtain the following systems, arranged according to the orders ε^j , $j = 1, 2, 3$

$$\begin{aligned} O(\varepsilon) : \mathbf{L}_c \begin{pmatrix} u_1 \\ v_1 \end{pmatrix} &= 0, \\ O(\varepsilon^2) : \mathbf{L}_c \begin{pmatrix} u_2 \\ v_2 \end{pmatrix} &= \begin{pmatrix} u_1^2 + cu_1 v_1 \\ bu_1 v_1 + v_1^2 \end{pmatrix}, \\ O(\varepsilon^3) : \mathbf{L}_c \begin{pmatrix} u_3 \\ v_3 \end{pmatrix} &= \frac{\partial}{\partial T} \begin{pmatrix} u_1 \\ v_1 \end{pmatrix} + \mu_2 k_c^\gamma \mathbf{M} \begin{pmatrix} u_1 \\ v_1 \end{pmatrix} \\ &\quad + \begin{pmatrix} 2u_1 u_2 + cu_1 v_2 + cu_2 v_1 \\ bu_1 v_2 + bu_2 v_1 + 2v_1 v_2 \end{pmatrix}. \end{aligned} \quad (3.3)$$

Our next goal is to describe the appearance of both diamonds and stripped spatial distributions as well as their spatio-temporal interactions. Since \mathbf{L}_c is the linear operator of the system at the Turing instability threshold, it holds that $(u_1, v_1)^T$ is the linear combination of the eigenvectors corresponding to the null eigenvalue. Therefore, at $O(\varepsilon)$ the solution of the system exhibits the following structure

$$\begin{pmatrix} u_1 \\ v_1 \end{pmatrix} = \begin{pmatrix} -K_1 \\ 1 \end{pmatrix} \sum_{j=1}^3 W_j \exp(i\mathbf{k}_j \cdot x) + c.c.,$$

where

$$K_1 = \frac{v^* + \sqrt{(1-bc)u^*v^*d_{22}/d_{11}}}{bv^*},$$

and W_j is the amplitude of the mode $\exp(i\mathbf{k}_j \cdot x)$ when the system is under the first-order perturbation. Its form is determined by the perturbation term of highest order. The addition of the complex conjugate *c.c.* allows $(u_1, v_1)^T$ to be real.

Next, we turn to the term of $O(\varepsilon^2)$. Since the right-hand side does not exhibit resonance-related terms, the solution is given simply by

$$\begin{pmatrix} u_2 \\ v_2 \end{pmatrix} = \begin{pmatrix} U_0 \\ V_0 \end{pmatrix} + \begin{pmatrix} U_j \\ V_j \end{pmatrix} \sum_{j=1}^3 \exp(i\mathbf{k}_j \cdot x) + c.c.$$

On the other hand, substitution of the above equation into the second equation of problem (3.3) yields

$$\begin{aligned} \mathbf{L}_c \begin{pmatrix} U_0 \\ V_0 \end{pmatrix} + \sum_{j=1}^3 \exp(i\mathbf{k}_j \cdot x) \mathbf{L}_c \begin{pmatrix} U_j \\ V_j \end{pmatrix} + \sum_{j=1}^3 \exp(-i\mathbf{k}_j \cdot x) \mathbf{L}_c \begin{pmatrix} \bar{U}_j \\ \bar{V}_j \end{pmatrix} \\ = (|W_1|^2 + |W_2|^2 + |W_3|^2) \begin{pmatrix} 2K_1^2 - 2cK_1 \\ 2 - 2bK_1 \end{pmatrix} + \sum_{j=1}^3 O(\exp(2i\mathbf{k}_j \cdot x)) \\ + O(\exp(i(\mathbf{k}_1 - \mathbf{k}_2) \cdot x)) + O(\exp(i(\mathbf{k}_2 - \mathbf{k}_3) \cdot x)) + O(\exp(i(\mathbf{k}_3 - \mathbf{k}_1) \cdot x)) + c.c., \end{aligned}$$

and after collecting terms of orders $O(1)$ and $O(\exp(i\mathbf{k}_j x))$, we obtain

$$\begin{pmatrix} U_0 \\ V_0 \end{pmatrix} = (|W_1|^2 + |W_2|^2 + |W_3|^2) \begin{pmatrix} -K_2 \\ 1 \end{pmatrix},$$

$$K_2 = \frac{v^{*2} + (v^* - 2)\sqrt{(1-bc)u^*v^*d_{22}/d_{11}}}{bv^{*2}}, \quad U_j = -K_1 V_j.$$

We now turn to the term of $O(\varepsilon^3)$. According to the Fredholm solvability condition, the vector function of the right-hand side must be orthogonal with the zero eigenvalues of the operator \mathbf{L}_c^+ in order to ensure the existence of a nontrivial solution to this equation, where \mathbf{L}_c^+ is the adjoint operator of \mathbf{L}_c . The nontrivial kernel of the operator \mathbf{L}_c^+ is

$$\begin{pmatrix} 1 \\ -K_3 \end{pmatrix} \exp(-i\mathbf{k}_j x), \quad K_3 = \frac{u^* + \sqrt{(1-bc)u^*v^*d_{11}/d_{22}}}{bv^*}.$$

Substituting the solution $(u_1, v_1)^T$ and $(u_2, v_2)^T$ into the problem containing the $O(\varepsilon^3)$ term, and applying Fredholm solvability condition, we can assert that

$$\begin{aligned} -(K_1 + K_3) \frac{\partial W_1}{\partial T} = & -\mu_2 k_c^\gamma W_1 - [2K_1(K_1 - c) - 2K_3(1 - bK_1)] (\bar{W}_2 \bar{V}_3 + \bar{V}_2 \bar{W}_3) \\ & - [2K_1 K_2 - cK_1 - cK_2 - K_3(2 - bK_1 - bK_2)] W_1 (|W_1|^2 \\ & + |W_2|^2 + |W_3|^2). \end{aligned} \quad (3.4)$$

In view of (3.1) and (3.2), the amplitude A_j^v can be expanded as

$$\begin{aligned} A_j^v &= \varepsilon W_j + \varepsilon^2 V_j + O(\varepsilon^3), \quad j = 1, 2, 3, \\ \partial_t A_j^v &= \varepsilon^3 \frac{\partial W_j}{\partial T} + O(\varepsilon^4). \end{aligned}$$

Multiplying (3.4) by $-\varepsilon^3$, we get

$$\begin{aligned} (K_1 + K_3) \partial_t A_1^v &= \varepsilon^2 \mu_2 k_c^\gamma A_1^v + [2K_1(K_1 - c) - 2K_3(1 - bK_1)] \bar{A}_2^v \bar{A}_3^v \\ &\quad - [cK_1 + cK_2 + K_3(2 - bK_1 - bK_2) \\ &\quad - 2K_1 K_2] A_1^v (|A_1^v|^2 + |A_2^v|^2 + |A_3^v|^2). \end{aligned} \quad (3.5)$$

In addition, multiplying (3.5) by $\frac{1}{k_c^\gamma d_{12}^c}$, we have the following amplitude equation

$$\tau_0 \partial_t A_1^v = \mu A_1^v + h \bar{A}_2^v \bar{A}_3^v - [g_1 |A_1^v|^2 + g_2 (|A_2^v|^2 + |A_3^v|^2)] A_1^v, \quad (3.6)$$

where $\mu = \frac{d_{12} - d_{12}^c}{d_{12}^c}$ is a normalized distance to the Turing instability threshold, and $\tau_0 = \frac{K_1 + K_3}{k_c^\gamma d_{12}^c}$ is a typical relaxation time. Moreover,

$$\begin{aligned} h &= \frac{2K_1(K_1 - c) - 2K_3(1 - bK_1)}{k_c^\gamma d_{12}^c}, \\ g_1 = g_2 &= \frac{cK_1 + cK_2 + K_3(2 - bK_1 - bK_2) - 2K_1 K_2}{k_c^\gamma d_{12}^c}. \end{aligned} \quad (3.7)$$

The remaining equations for A_2^v and A_3^v can be obtained analogously, through transformation of the subscript of A^v .

In order to study the pattern selection, we need to analyze further the amplitude Eq. (3.6), where each amplitude can be decomposed into a mode $\rho_j = |A_j^v|$ and a corresponding phase angle φ_j . We proceed to rewrite (3.6) and the other two associated amplitude equations for $A_j^v = \rho_j \exp(i\varphi_j)$ in the following form:

$$\tau_0 \partial_t \Phi = -h \frac{\rho_1^2 \rho_2^2 + \rho_1^2 \rho_3^2 + \rho_2^2 \rho_3^2}{\rho_1 \rho_2 \rho_3} \sin \Phi, \quad (3.8)$$

$$\begin{aligned}\tau_0 \partial_t \rho_1 &= \mu \rho_1 + h \rho_2 \rho_3 \cos \Phi - g_1 \rho_3 - g_2 (\rho_2^2 + \rho_3^2) \rho_1, \\ \tau_0 \partial_t \rho_2 &= \mu \rho_2 + h \rho_1 \rho_3 \cos \Phi - g_1 \rho_2 - g_2 (\rho_1^2 + \rho_3^2) \rho_2, \\ \tau_0 \partial_t \rho_3 &= \mu \rho_3 + h \rho_1 \rho_2 \cos \Phi - g_1 \rho_1 - g_2 (\rho_1^2 + \rho_2^2) \rho_3,\end{aligned}$$

where $\Phi = \phi_1 + \phi_2 + \phi_3$. The above equations imply that when the system is at steady state, the sum of the amplitude-phases only attains two values $\Phi = 0$ and $\Phi = \pi$. The fact that $\rho_j > 0$ for $j = 1, 2, 3$, implies that in the case $\Phi = 0$, the solutions of Eq. (3.8) are stable when $h > 0$; whereas for $\Phi = \pi$, the solutions of Eq. (3.8) are stable when $h < 0$. If we consider only the stable solutions of Eq. (3.8), then the mode equations can be recast in the form:

$$\tau_0 \frac{d\rho_1}{dt} = \mu \rho_1 + |h| \rho_2 \rho_3 - g_1 \rho_1^3 - g_2 (\rho_2^2 + \rho_3^2) \rho_1, \quad (3.9)$$

$$\tau_0 \frac{d\rho_2}{dt} = \mu \rho_2 + |h| \rho_1 \rho_3 - g_1 \rho_2^3 - g_2 (\rho_1^2 + \rho_3^2) \rho_2, \quad (3.10)$$

$$\tau_0 \frac{d\rho_3}{dt} = \mu \rho_3 + |h| \rho_1 \rho_2 - g_1 \rho_3^3 - g_2 (\rho_1^2 + \rho_2^2) \rho_3. \quad (3.11)$$

Notice that the quadratic terms in (3.9)–(3.11) are positive, which is the main cause of instability in the linear term. In order to ensure that mode equations possess a steady state solution, the coefficients of cubic terms must be positive, which translates in imposing the following conditions

$$cK_1 + cK_2 + K_3(2 - bK_1 - bK_2) > 2K_1 K_2,$$

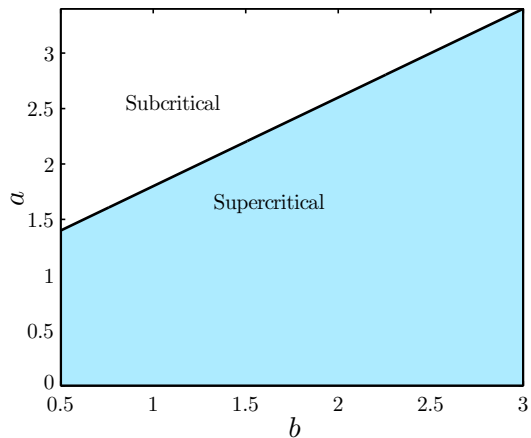
that in turn yield super-critical Turing bifurcations in system (1.1). Otherwise, the weakly nonlinear analysis requires to be extended by expanding the Taylor series in (3.3) up to the fifth order so that the instability is covered [that is, (3.8) holds]. The latter case corresponds to the so-called sub-critical Turing bifurcation, which we do not consider in the present paper. Figure 3 displays the Turing bifurcation diagram in the (b, a) plane.

In order to assess the stability of the mode equations, we add a perturbation $(\delta\rho_1, \delta\rho_2, \delta\rho_3)$ to the steady state (ρ_1, ρ_2, ρ_3) and substitute it into Eqs. (3.9)–(3.11). Retaining the linear terms, we end up with the linear perturbation equations:

$$\begin{aligned}\tau_0 \frac{d}{dt} \begin{pmatrix} \delta\rho_1 \\ \delta\rho_2 \\ \delta\rho_3 \end{pmatrix} &= \mathbf{J} \begin{pmatrix} \delta\rho_1 \\ \delta\rho_2 \\ \delta\rho_3 \end{pmatrix}, \\ \text{where } \mathbf{J} &= \begin{pmatrix} \mu - 3g_1\rho_1^2 - g_2(\rho_2^2 + \rho_3^2) & |h|\rho_3 - 2g_2\rho_1\rho_2 & |h|\rho_2 - 2g_2\rho_1\rho_3 \\ |h|\rho_3 - 2g_2\rho_1\rho_2 & \mu - 3g_1\rho_2^2 - g_2(\rho_1^2 + \rho_3^2) & |h|\rho_1 - 2g_2\rho_2\rho_3 \\ |h|\rho_2 - 2g_2\rho_1\rho_3 & |h|\rho_1 - 2g_2\rho_2\rho_3 & \mu - 3g_1\rho_3^2 - g_2(\rho_1^2 + \rho_2^2) \end{pmatrix}.\end{aligned} \quad (3.12)$$

We now focus on the stability of Turing patterns, for which we separate the discussion into two cases depending on the shape of the spatial distributions.

Fig. 3 Turing bifurcation diagram. The *shaded region* represents the super-critical states, whereas the *white region* is sub-critical zone. The remaining parameters are $c = 0.2$, $d_{11} = 1$, and $d_{22} = 1$



Case (I) Striped patterns correspond to

$$(\rho_1, \rho_2, \rho_3) = (\rho, 0, 0), \text{ where } \rho = \sqrt{\mu/g_1}. \quad (3.13)$$

Substituting (3.13) into the perturbation Eq. (3.12), we have

$$\tau_0 \frac{d}{dt} \begin{pmatrix} \delta\rho_1 \\ \delta\rho_2 \\ \delta\rho_3 \end{pmatrix} = \begin{pmatrix} -2\mu & 0 & 0 \\ 0 & \mu(1-g_2/g_1) & |h|\sqrt{\mu/g_1} \\ 0 & |h|\sqrt{\mu/g_1} & \mu(1-g_2/g_1) \end{pmatrix} \begin{pmatrix} \delta\rho_1 \\ \delta\rho_2 \\ \delta\rho_3 \end{pmatrix}. \quad (3.14)$$

In view of $g_1 = g_2$ defined in (3.7), we have that the three eigenvalues of system (3.14) are

$$\lambda_1 = -2\mu < 0, \lambda_2 = -|h|\sqrt{\mu/g_1} < 0, \lambda_3 = |h|\sqrt{\mu/g_1} > 0,$$

and therefore striped patterns are not stable and will eventually vanish in the long term.

Case (II) Diamond-shaped patterns correspond to

$$(\rho_1, \rho_2, \rho_3) = (\rho, \rho, \rho), \text{ where } \rho = \frac{|h| \pm \sqrt{h^2 + 4(g_1 + 2g_2)\mu}}{2(g_1 + 2g_2)}. \quad (3.15)$$

Substituting (3.15) into the perturbation Eq. (3.12), we have

$$\tau_0 \frac{d}{dt} \begin{pmatrix} \delta\rho_1 \\ \delta\rho_2 \\ \delta\rho_3 \end{pmatrix} = \begin{pmatrix} \alpha & \beta & \beta \\ \beta & \alpha & \beta \\ \beta & \beta & \alpha \end{pmatrix} \begin{pmatrix} \delta\rho_1 \\ \delta\rho_2 \\ \delta\rho_3 \end{pmatrix}, \quad (3.16)$$

where $\alpha = \mu - 5g_1\rho^2$, $\beta = |h|\rho - 2g_1\rho^2$. The characteristic equation of (3.16) is

$$(\lambda - \alpha)^3 - 3\beta^2(\lambda - \alpha) - 2\beta^3 = 0,$$

and so the three eigenvalues of system (3.14) are

$$\lambda_1 = \lambda_2 = \mu - |h|\rho - 3g_1\rho^2, \quad \lambda_3 = \mu + 2|h|\rho - 9g_1\rho^2. \quad (3.17)$$

Substituting $\rho = \frac{|h| \pm \sqrt{h^2 + 4(g_1 + 2g_2)\mu}}{2(g_1 + 2g_2)}$ and $g_1 = g_2$ into (3.17), we have

$$\lambda_1 = \lambda_2 = -\frac{h^2}{3g_1} < 0, \quad \lambda_3 = -\frac{12g_1\mu + h^2 \pm |h|\sqrt{h^2 + 12g_1\mu}}{6g_1} < 0.$$

Therefore, diamond-shaped patterns are stable whenever $\mu > -\frac{h^2}{12g_1}$.

4 Numerical examples and finite volume method and multiresolution-based adaptivity

4.1 Preliminaries and admissible meshes

Let us consider a discretization of the time interval $(0, T)$ by setting $t^n := n\Delta t$ for $n \in \{0, \dots, N\}$, where N is the smallest integer such that $N\Delta t \geq T$. By an *admissible mesh* for Ω we will refer to a family \mathcal{T} of control volumes of maximum diameter h and a family of points $(x_K)_{K \in \mathcal{T}}$ satisfying the following properties (cf. Eymard et al. 2000, Def. 5.1). For a given finite volume $K \in \mathcal{T}$, x_K is its center and $N(K)$ the set of its neighbors (control volumes sharing a common edge with K). We denote by $\mathcal{E}(K)$ the set of edges of K , $\mathcal{E}_{\text{int}}(K)$ is the restriction to those in the interior of Ω and $\mathcal{E}_{\text{ext}}(K) = \mathcal{E}(K) \setminus \mathcal{E}_{\text{int}}(K)$ is the set of edges of K lying on $\partial\Omega$. For every $L \in N(K)$, by $\sigma = K|L$ ($\sigma = K|\partial\Omega$, respectively) we denote the interface between K and L (between K and $\partial\Omega$, respectively). By $\mathbf{n}_{K,\sigma}$ we denote the unit normal vector to $\sigma = K|L$ ($\sigma \in \mathcal{E}_{\text{ext}}(K)$, respectively) pointing from K to L (from K to $\partial\Omega$, respectively). Moreover, $|K|$ stands for the two-dimensional measure of K and $|\sigma|$ for the one-dimensional measure of $\sigma \in \mathcal{E}$. It is also assumed that

$$\text{The segment } \overline{x_K x_L} \text{ is orthogonal to } \sigma_{K,L} \text{ for every } K, L \in \mathcal{T}. \quad (4.1)$$

4.2 Multiresolution setting

We now introduce a hierarchy of nested admissible meshes $\mathcal{T}^0 \subset \dots \subset \mathcal{T}^H$ forming a graded tree Λ , in which each grid \mathcal{T}^l is a compound of control volumes K^l of the level l , $l = 0, \dots, H$, where $l = 0$ corresponds to the coarsest and $l = H$ to the finest level of the tree Λ . In order to define a multiresolution framework (Berres and Ruiz-Baier 2011), for a given control volume K^l we define a refinement set by

$$\mathcal{R}_{K^l} := \{L_i^{l+1}\}_i,$$

where L_i^{l+1} denotes a control volume at the resolution level $l + 1$, $L_i^{l+1} \subset K^l$. By definition of the nested hierarchy, it holds that

$$\overline{K^l} := \bigcup_{i=1}^{\#\mathcal{R}_{K^l}} L_i^{l+1}.$$

For $\mathbf{x} \in K^l$ the *scale box function* is defined as $\varphi_{K^l}(\mathbf{x}) := |K^l|^{-1} \chi_{K^l}(\mathbf{x})$ (where χ is the characteristic function), and therefore the average of any function $w(t) \in L^1(\Omega)$ over K^l can be recast as $w_{K^l}(t) = \langle w(t), \varphi_{K^l} \rangle_{L^1(\Omega)}$.

To move between resolution levels, certain transfer operators are needed. With the help of these maps, one can determine an invertible transformation between finite volumes on level $l = H$, and the set formed by finite volumes on the level $l = 0$ and a sequence of *wavelet coefficients*. To switch from fine to coarser levels, a projection operator for cell averages and box functions is defined by

$$w(t)_{K^l} = \sum_{L_i^{l+1} \in \mathcal{R}_{K^l}} \frac{|L_i^{l+1}|}{|K^l|} w(t)_{L_i^{l+1}}, \quad \varphi_{K^l} = \sum_{L_i^{l+1} \in \mathcal{R}_{K^l}} \frac{|L_i^{l+1}|}{|K^l|} \varphi_{L_i^{l+1}},$$

whereas to move from coarse to fine levels we define a polynomial interpolation

$$\tilde{w}(t)_{K^{l+1}} = \sum_{T^l \in \mathcal{S}_K^l} g_{K,T}^l w(t)_{T^l}.$$

The set \mathcal{S}_K^l is a stencil of interpolation (of order s), and $g_{K,T}^l$ are prediction coefficients. Further details on the precise definition of these coefficients and stencils are given in e.g. [Bendahmane et al. \(2009\)](#). For $\mathbf{x} \in K^{l+1}$, and depending on the choice of the predictor map, the *wavelet function* is defined as

$$\psi_{K^l,j} = \varphi_{L_i^{l+1}} - \sum_{m=-s}^s \tilde{\gamma}_{i+m} \varphi_{L_{i+m}^l} \quad \text{for } j = 1, \dots, \#\mathcal{R}_{K^l},$$

where $L_i^{l+1} \in \mathcal{R}_{K^l}$, and the value of each $\tilde{\gamma}_{i+m}$ depends on the coefficients $g_{K,T}^l$ of the prediction operator. The difference between the cell average and the predicted value for the scalar $w(t)$ is called wavelet coefficient and is defined by

$$d_{K^l}^w := |w(t)_{K^l} - \tilde{w}(t)_{K^l}| = |\langle w(t), \psi_{K^l} \rangle|.$$

Data compression is achieved by discarding all information of control volumes where the local wavelet coefficient is lower than a level-dependent tolerance, i.e.,

$$d_{K^l}^w < \varepsilon_l, \quad l = 0, \dots, H. \tag{4.2}$$

These level-dependent tolerances can be defined so that the error due to thresholding is of the same order as the discretization error induced by the baseline finite volume formulation, therefore preserving the order of the base scheme ([Berres and Ruiz-Baier 2011](#)).

Remark 1 The key concept of the fully adaptive strategy of multiresolution consists in defining an evolving set of leaves $\mathcal{L}(\Lambda)$ of the tree Λ , formed by all tree nodes K^l that are not discarded by the thresholding defined in (4.2), and such that all cells in \mathcal{R}_{K^l} satisfy (4.2). Then, the underlying discrete scheme is first defined on $\mathcal{L}(\Lambda)$. However, $\mathcal{L}(\Lambda)$ is not an admissible mesh in general, and therefore an auxiliary set of nodes, called *virtual leaves* is required in order to fulfill (4.1).

The set of virtual leaves consists in cells of $\Lambda \setminus \mathcal{L}(\Lambda)$ that for a given $K^l \in \mathcal{L}(\Lambda)$, belong to $N(K^l) \cap \mathcal{T}^l$. We will denote by $\tilde{\mathcal{L}}(\Lambda)$ the set formed by leaves and virtual leaves. In addition, the set Λ_d of cells marked as *deletable* consists in all elements that satisfy (4.2). Virtual leaves are needed to evaluate numerical fluxes on each leaf.

4.3 Multiresolution: finite volume formulation

The baseline finite volume discretization of (1.2) is based on the so-called shifted Grünwald approximation of local gradients (see e.g. [Meerschaert and Tadjeran 2006](#); [Yang et al. 2010](#)). Irrespective of the specific form of the gradient approximation, the property of local flux conservation yields the following expression for a first order finite volume approximation of the fractional diffusion operator applied to a generic scalar field w over the finest-level cell K^H at time t^n :

$$-\widetilde{\Delta^{\gamma/2}} := -\Delta^{\gamma/2} w_{K^H}^n \approx - \sum_{L_i \in \mathcal{H}(K^H)} g_{\gamma, L_i} \frac{|\sigma_{K^H, L_i}|}{d_{K^H, L_i}} (w_{L_i}^n - w_{K^H}^n), \quad (4.3)$$

where g_{γ, L_i} , \mathcal{H} are, respectively, particular weights and approximation stencil which we will precisely defined in terms of Cartesian grids, for sake of clarity. Let us assume a square domain Ω discretized into $N_x \times N_y$ equally sized boxes of area $h_x h_y$, and notice that (4.3) can be written as

$$-\widetilde{\Delta^{\gamma/2}} w_{ij}^n = -\frac{1}{h_x^\gamma} \sum_{k=0}^{i+1} g_{\gamma, k} w_{i-k+1, j}^n - \frac{1}{h_y^\gamma} \sum_{l=0}^{j+1} g_{\gamma, l} w_{i, j-l+1}^n,$$

where $g_{\gamma, m} := (-1)^m \binom{\gamma}{m}$, (see also [Concezzi and Spigler 2012](#)). These considerations imply that the fully explicit Euler FV discrete analogue of (1.2) defined on the finest mesh reads: Starting from a L^2 -average of the initial data

$$u_{K^H}^0 = \frac{1}{|K^H|} \int_{K^H} u_0(x) dx, \quad v_{K^H}^0 = \frac{1}{|K^H|} \int_{K^H} v_0(x) dx, \quad \forall K^H \in \mathcal{T}^H,$$

and for every $n = 0, \dots$, recursively find $u_{K^H}^{n+1}, v_{K^H}^{n+1}$ such that

$$\begin{aligned} |K^H| \frac{u_{K^H}^{n+1} - u_{K^H}^n}{\Delta t} - d_{11} \widetilde{\Delta^{\gamma/2}} u_{K^H}^n - d_{12} \widetilde{\Delta^{\gamma/2}} v_{K^H}^n &= |K| F_{K^H}^n, \\ |K^H| \frac{v_{K^H}^{n+1} - v_{K^H}^n}{\Delta t} - d_{22} \widetilde{\Delta^{\gamma/2}} v_{K^H}^n &= |K| G_{K^H}^n, \end{aligned} \quad (4.4)$$

where $F_{K^H}^n, G_{K^H}^n$ are explicit approximations of the reaction terms over each control volume

$$\frac{1}{|K^H|} \int_K F(u(x, t^n), v(x, t^n)) dx, \quad \frac{1}{|K^H|} \int_K G(u(x, t^n), v(x, t^n)) dx,$$

and are given by

$$F_{K^H}^n = F(u_{K^H}^n^+, v_{K^H}^n^+), \quad G_{K^H}^n = G(u_{K^H}^n^+, v_{K^H}^n^+).$$

We stress that if K^l is a leaf, then the unknowns are computed from the MRFV method (4.4), whereas if K^l is a virtual leaf, the values of each species concentration are simply obtained by the MR transform of their values at lower refinement levels.

4.4 Numerical examples

For numerically studying the pattern formation of system (1.1), it suffices to consider the dynamics induced by small-amplitude perturbations to the homogeneous steady state. The domain is confined to the square $\Omega = [0, 10] \times [0, 10]$, and it is discretized using a Cartesian mesh consisting of 262, 144 cells in the highest resolution level $H = 9$, and the time step is $\Delta t = 0.0025$. As in Sect. 2, the model parameters are set to $\gamma = 1, a = 2.5, b = 1.5, c = 0.2, d_{11} = d_{22} = 1, d_{12} = 1.8$, and the reference tolerance required for the thresholding algorithm is fixed to $\varepsilon_R = 0.0001$. The initial data is taken as

$$u(x, 0) = u^* + \eta_1(x), \quad v(x, 0) = v^* + \eta_2(x), \quad (4.5)$$

where $\eta_1 \in [-0.05, 0.05]$ and $\eta_2 \in [-0.025, 0.025]$ are uniformly distributed random perturbations and (u^*, v^*) is the equilibrium state. No-flux boundary conditions are applied for each problem, representing that the species do not leave the domain. The time evolution (snapshots at early, moderate, and advanced times) of the perturbed initial state (4.5) is displayed in Fig. 4, where we can observe convergence to diamond-shaped spatial patterns. Note that in the case of normal diffusion, the system is expected to exhibit a regime of self-replicating spots, as discussed in e.g. Pearson (1993). We also depict sketches of the meshes generated by the multiresolution strategy (see the bottom row of Fig. 4), which after successive local refinement and coarsening clearly identify the zones of high solution gradients. The multiresolution method also allows substantial reduction in computational burden due to the fast MR transform and graded

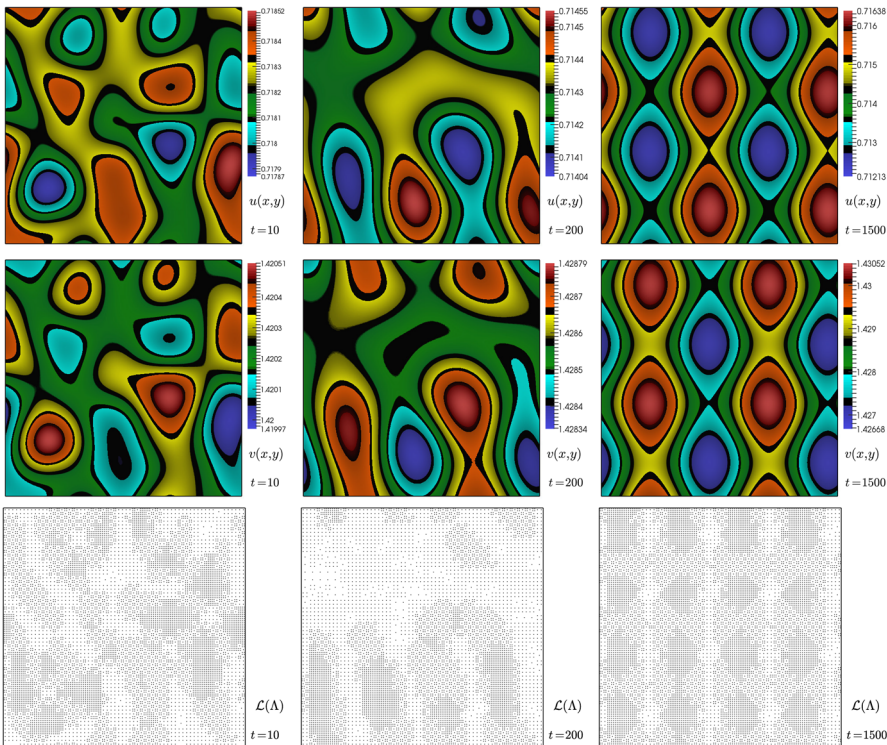


Fig. 4 Snapshots at $t = 10, 200, 1500$ (left, center, right, respectively) of the Turing pattern formation for species u, v (top and middle, respectively) in the case where the order of Weyl fractional operator is $\gamma = 1$. The employed parameters are $a = 2.5, b = 1.5, c = 0.2, d_{11} = d_{22} = 1, d_{12} = 1.8$. The bottom panels exhibit snapshots of the mass center of leaves in the adaptively refined meshes generated with the multiresolution algorithm with a global threshold of $\varepsilon_R = 0.0001$

tree structure (Bendahmane et al. 2009). We also present an analogous test where we have only modified the order of the fractional diffusion to $\gamma = 1.5$, and we can observe some differences in terms of spatial distribution of patterns. The approximate solutions along with fully adaptive meshes are presented in Fig. 5. In particular we observe a faster arrangement of spatial structures than those shown in Fig. 4.

In addition, the amplitude of the modes in the two-dimensional k -space can be observed employing the amplitude spectrum of the solution, computed as follows for a generic scalar field w_h :

$$\mathcal{S}(w_h) := \log \left\{ \left| \mathcal{J}_0(\mathcal{F}_h(w_h)) \right| \right\},$$

where \mathcal{F}_h denotes the two-dimensional discrete Fourier transform and \mathcal{J}_0 is a shift operator that translates the zero frequency component to the center of the spectrum. Figure 6 depicts these spectra for the solutions of both tests displayed in Figs. 4 and 5.

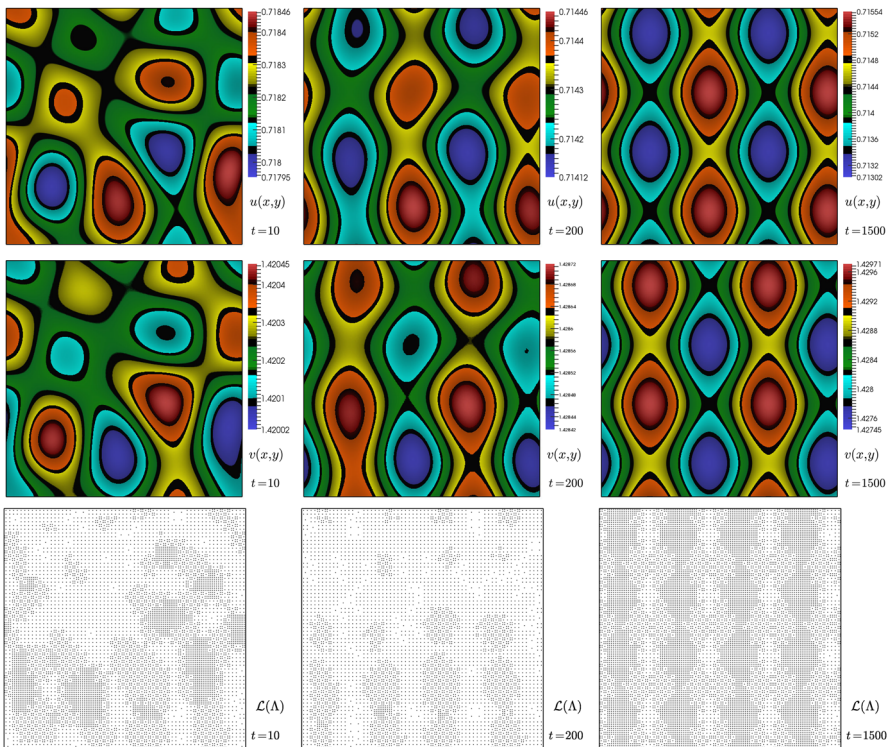


Fig. 5 Snapshots at $t = 10, 200, 1500$ (left, center, right, respectively) of the Turing pattern formation for species u, v (top and middle, respectively) in the case where the order of Weyl fractional operator is $\gamma = 1.5$. The remaining parameters are chosen as in the previous example. The bottom panels show snapshots of the mass center of leaves in the adaptively refined meshes generated with the multiresolution algorithm with a global threshold of $\varepsilon_R = 0.0001$

5 Concluding remarks

We have introduced the Lévy flights type of super-diffusion into a Lotka-Volterra competitive model, which means that the species jump length has a heavy tailed distribution. Even if pattern formation studies for the super-diffusive reaction diffusion system are numerous (Viswanathan et al. 1996; Schmitt and Seuront 2001; Toner et al. 2005), up to the authors' knowledge, the specific role of super cross-diffusion has not been studied in detail. Our results show that without super cross-diffusion, the system lacks of an inhomogeneous steady state. In contrast, the presence of super cross-diffusion drives the onset of Turing instabilities. We have determined a threshold value for the super cross-diffusion coefficient, in order to determine the stability of Turing patterns. Comparing sub-diffusive with normal diffusive models, we conclude that changes occur not only regarding the shapes of the obtained Turing patterns, but also on the wavenumber: that of sub-diffusive models is less than the one in

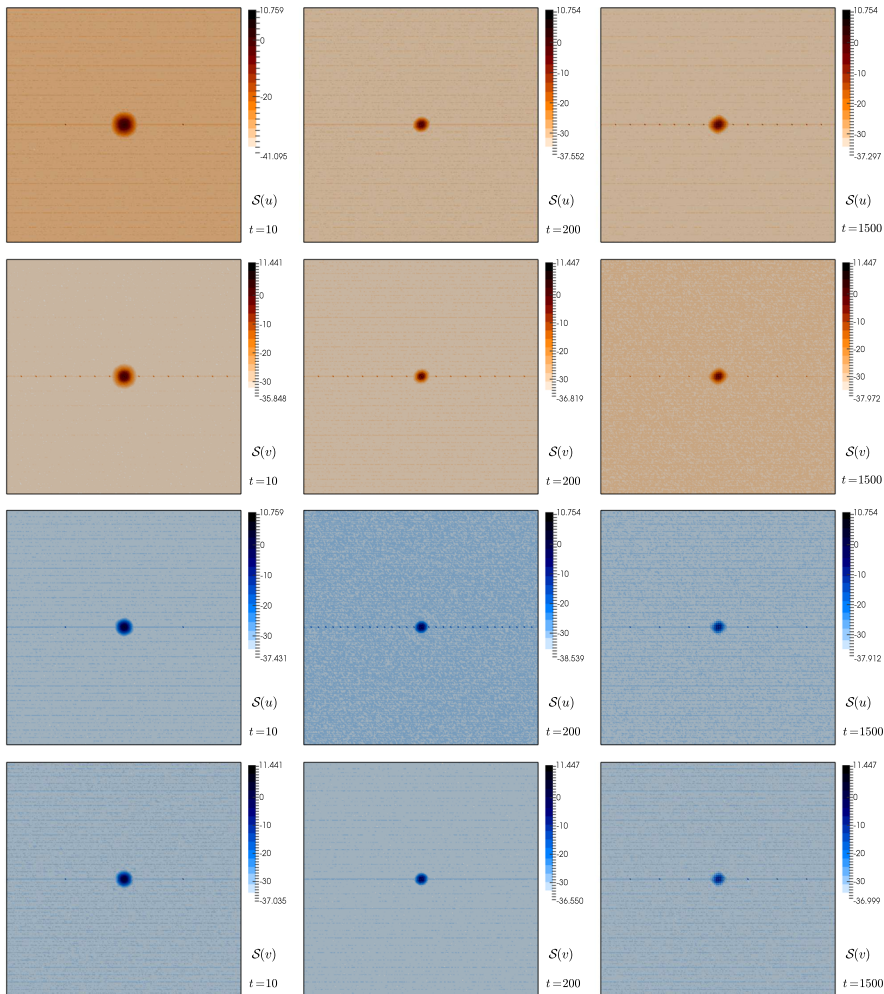


Fig. 6 Snapshots at $t = 10, 200, 1500$ (left, center, right, respectively) of the Fourier spectrum of species u, v in the case where the order of Weyl fractional operator is $\gamma = 1$ (top figures) or $\gamma = 1.5$ (last two rows)

normal diffusive models. An immediate application of these observations from the viewpoint of biology, is that when the inter-population competition is larger than the intra-population competition, the reached inhomogeneous steady state is stable.

Acknowledgments RRB gratefully acknowledges the support by the Swiss National Science Foundation through the research Grant PP00P2_144922; and CT acknowledges partial support by the PRC Grant NSFC 11201406 and by the Qinglan Project. Finally, we thank the helpful remarks by an anonymous referee, which resulted in substantial improvements to the initial version of this manuscript.

Appendix

In this appendix we sketch an existence proof for the fractional reaction-diffusion system (1.2). Note that in [Baeumer et al. \(2007\)](#), the authors study a fractional equation

of type $\partial_t u = \nabla^\gamma u + f(u)$. They prove existence of so-called mild solutions (the solution in the sense of semi-group theory) by assuming f Lipschitz continuous and a more regular initial condition u_0 . In comparison to Baeumer et al. (2007), our proof is based on introducing an approximation system to which we can apply the Faedo-Galerkin scheme. To prove convergence to weak solutions of the approximate solutions we utilize monotonicity and compactness methods. Moreover, since our weak solution (u, v) is only bounded in L^2 (because the initial datum (u_0, v_0) is only bounded in L^2), then the source terms are not Lipschitz continuous (they are nonlinear functions in u and v).

Let Ω be a bounded open subset of \mathbf{R}^d ($d = 2, 3$) with a smooth (say C^2) boundary $\partial\Omega$. For $1 \leq q < \infty$ and X is a Banach space, then $L^q(0, T; X)$ denotes the space of measurable function $u : (0, T) \rightarrow X$ for which $t \mapsto \|u(t)\|_X \in L^q(0, T)$. Moreover, $C([0, T]; X)$ denotes the space of continuous functions $u : [0, T] \rightarrow X$ for which $\|u\|_{C([0, T]; X)} := \max_{t \in (0, T)} \|u(t)\|_X$ is finite.

The Fourier transform \hat{u} of a tempered distribution $u(x)$ on Ω is defined by

$$\hat{u}(\mathbf{k}) = \frac{1}{(2\pi)^d} \int_{\Omega} \exp(-i\mathbf{k} \cdot x) u(x) dx.$$

Note that the fractional diffusion operator Λ^γ can be identified with the Fourier transform

$$\widehat{\Lambda^\gamma u}(\mathbf{k}) = |i\mathbf{k}|^\gamma \hat{u}(\mathbf{k}),$$

for $\gamma \in \mathbf{R}$. We denote by $H^\gamma(\Omega)$ the non-homogeneous fractional Sobolev space of functions u such that

$$\|u\|_{H^\gamma(\Omega)} = \left(\sum_{\mathbf{k} \in \mathbf{Z}^d} \left(1 + |\mathbf{k}|^2\right)^\gamma |\hat{u}(\mathbf{k})|^2 \right)^{\frac{1}{2}} < \infty.$$

The homogeneous fractional Sobolev space of functions u is denoted by $\tilde{H}^\gamma(\Omega)$ given by

$$\|u\|_{\tilde{H}^\gamma(\Omega)} = \left(\sum_{\mathbf{k} \in \mathbf{Z}^d} |\mathbf{k}|^{2\gamma} |\hat{u}(\mathbf{k})|^2 \right)^{\frac{1}{2}} < \infty.$$

Next, we define $-\Delta : H^1(\Omega) \rightarrow L^2(\Omega)$ with domain:

$$\text{Dom}(-\Delta) = \left\{ u \in H^1(\Omega) \text{ such that } \Delta u \in L^2(\Omega) \right\}.$$

Note that the operator $A = -\Delta$ is positive, unbounded, closed and its inverse is compact. This implies

$$Aw_\ell = \lambda_\ell w_\ell,$$

for $w_\ell \in \text{Dom}(-\Delta)$, where $\{w_\ell\}_{\ell=1}^\infty$ are the eigenfunctions (orthogonal basis of $H^1(\Omega)$) with the corresponding eigenvalues $\{\lambda_\ell\}_{\ell=1}^\infty$.

With this spectral decomposition the fractional powers of the fractional Laplacian Λ^γ ($\Lambda = (-\Delta)^{1/2}$, $1 < \gamma \leq 2$) can be defined for $u \in C^\infty(\Omega)$ by

$$(-\Delta)^{\gamma/2}u = \Lambda^\gamma u = \sum_{\ell=1}^{\infty} u_\ell \lambda_\ell^{\gamma/2} w_\ell$$

where the coefficients u_ℓ are defined by $u_\ell = \int_{\Omega} u w_\ell$.

Now we define what we mean by weak solutions of the system (1.2) completed with Neumann boundary conditions and initial conditions on u, v :

Definition 5.1 A weak solution of (1.2) is a set of nonnegative functions (u, v) such that,

- (a) $(u, v) \in L^\infty(0, T; L^2(\Omega, \mathbf{R}^d)) \cap L^2(0, T; \tilde{H}^{\gamma/2}(\Omega, \mathbf{R}^d))$,
- (b) $F(u, v), G(u, v) \in L^1((0, T) \times \Omega)$, $u(0, \cdot) = u_0(\cdot)$ and $v(0, \cdot) = v_0(\cdot)$ a.e. in Ω ,
- (c) $Q_T = \Omega \times [0, T]$ and they satisfy

$$\begin{aligned} & - \iint_{Q_T} u \partial_t \varphi_1 \, dx \, dt + d_{11} \iint_{\Omega} \Lambda^{\gamma/2} u \cdot \Lambda^{\gamma/2} \varphi_1 \, dx \, dt \\ & + d_{12} \iint_{\Omega} \Lambda^{\gamma/2} v \cdot \Lambda^{\gamma/2} \varphi_1 \, dx \, dt \\ & = - \int_{\Omega} u_0(x) \varphi_1(0, x) \, dx + \iint_{Q_T} F(u, v) \varphi_1 \, dx \, dt, \\ & - \iint_{Q_T} v \partial_t \varphi_2 \, dx \, dt + d_{22} \iint_{\Omega} \Lambda^{\gamma/2} v \cdot \Lambda^{\gamma/2} \varphi_2 \, dx \, dt \\ & = - \int_{\Omega} v_0(x) \varphi_2(0, x) \, dx + \iint_{Q_T} G(u, v) \varphi_2 \, dx \, dt, \end{aligned}$$

for all $\varphi_1, \varphi_2 \in \mathcal{D}([0, T) \times \Omega)$, where $F(u, v) = u(1 - u - cv)$ and $G(u, v) = v(a - bu - v)$.

Theorem 1 If $(u_0, v_0) \in L^2(\Omega, \mathbf{R}^d)$, then problem (1.2) possesses a weak solution in the sense of Definition 5.1.

The proof of Theorem 1 (the existence of weak solution) is based on Faedo-Galerkin method. Although the existence proof for (1.2) will be the subject of a separate contribution, we outline in what follows the main steps. We look for finite dimensional approximate solution to the problem (1.2) [we complete the system (1.2) with Neumann boundary conditions and initial conditions on u, v]: as sequences $(u_n)_{n>1}, (v_n)_{n>1}$ defined for $t \geq 0$ and $x \in \overline{\Omega}$ by

$$u_n(t, x) = \sum_{l=1}^n b_{n,l}(t) w_l(x), \quad v_n(t, x) = \sum_{l=1}^n c_{n,l}(t) w_l(x). \quad (5.1)$$

The next step is to determine the coefficients $(b_{n,l}(t))_{l=1}^n, (c_{n,l}(t))_{l=1}^n$ such that for $k = 1, \dots, n$ it holds

$$\begin{aligned} & (\partial_t u_n, w_k)_{L^2(\Omega)} + d_{11} \int_{\Omega} \Lambda^{\gamma/2} u_n \cdot \Lambda^{\gamma/2} w_k dx + d_{12} \int_{\Omega} \Lambda^{\gamma/2} v_n \cdot \Lambda^{\gamma/2} w_k dx \\ &= \int_{\Omega} F(u_n^+, v_n^+) w_k dx, (\partial_t v_n, w_k)_{L^2(\Omega)} + d_{22} \int_{\Omega} \Lambda^{\gamma/2} v_n \cdot \Lambda^{\gamma/2} w_k dx \\ &= \int_{\Omega} G(u_n^+, v_n^+) w_k dx, \end{aligned} \quad (5.2)$$

and regarding to the initial conditions,

$$\begin{aligned} u_n(0, x) &= u_{0,n}(x) := \sum_{l=1}^n b_{n,l}(0) w_l(x), \quad b_{n,l}(0) := (u_0, w_l)_{L^2(\Omega)}, \\ v_n(0, x) &= v_{0,n}(x) := \sum_{l=1}^n c_{n,l}(0) w_l(x), \quad c_{n,l}(0) := (v_0, w_l)_{L^2(\Omega)}. \end{aligned}$$

Herein

$$F(u_n^+, v_n^+) = u_n^+ (1 - u_n^+ - c v_n^+) \text{ and } G(u_n^+, v_n^+) = v_n^+ (a - b u_n^+ - v_n^+),$$

where $w^+ = \max(0, -w)$ for $w = u, v$.

Observe that, since $u_0, v_0 \in L^2(\Omega)$, it is clearly seen that as $n \rightarrow \infty$, $u_{0,n} \rightarrow u_0$ and $v_{0,n} \rightarrow v_0$ in $L^2(\Omega)$, respectively. Using the normality of the respective basis, we can write (5.2) as a system of ordinary differential equations:

$$\begin{aligned} & b'_{n,k}(t) + d_{11} \int_{\Omega} \Lambda^{\gamma/2} u_n \cdot \Lambda^{\gamma/2} w_k dx + d_{12} \int_{\Omega} \Lambda^{\gamma/2} v_n \cdot \Lambda^{\gamma/2} w_k dx \\ &= \int_{\Omega} F(u_n^+, v_n^+) w_k dx, c'_{n,k}(t) + d_{22} \int_{\Omega} \Lambda^{\gamma/2} v_n \cdot \Lambda^{\gamma/2} w_k dx \\ &= \int_{\Omega} G(u_n^+, v_n^+) w_k dx. \end{aligned}$$

Let \mathcal{F} and \mathcal{G} be functions defined as follow:

$$\begin{aligned} \mathcal{F}(t, (b_{n,l}(t))_{l=1}^n, (c_{n,l}(t))_{l=1}^n) &:= \int_{\Omega} F(u_n^+, v_n^+) w_k dx - d_{11} \int_{\Omega} \Lambda^{\gamma/2} u_n \cdot \Lambda^{\gamma/2} w_k dx \\ &\quad - d_{12} \int_{\Omega} \Lambda^{\gamma/2} v_n \cdot \Lambda^{\gamma/2} w_k dx, \\ \mathcal{G}(t, (b_{n,l}(t))_{l=1}^n, (c_{n,l}(t))_{l=1}^n) &:= \int_{\Omega} G(u_n^+, v_n^+) w_k dx - d_{22} \int_{\Omega} \Lambda^{\gamma/2} v_n \cdot \Lambda^{\gamma/2} w_k dx. \end{aligned}$$

Proceeding in an analogous way to the developments in Andreianov et al. (2011), Bendahmane (2010) and Bendahmane and Karlsen (2006), we can prove that \mathcal{F} and

\mathcal{G} are Carathéodory functions, and we can show an existence interval $[0, t')$ for the Faedo-Galerkin solutions u_n and v_n defined by (5.1).

On the other hand, to prove global existence of the solutions we derive n -independent a priori estimates bounding u_n, v_n in various Banach spaces. Given some continuous coefficients $d_{1,n,l}(t)$ and $d_{2,n,l}(t)$, we form the functions $\varphi_{1,n}(t, x) := \sum_{l=1}^n d_{1,n,l}(t) w_l(x)$ and $\varphi_{2,n}(t, x) := \sum_{l=1}^n d_{2,n,l}(t) w_l(x)$. Now our Faedo-Galerkin solutions satisfy the following weak formulations:

$$\begin{aligned} & \int_{\Omega} \partial_s u_n \varphi_{1,n} dx + d_{11} \int_{\Omega} \Lambda^{\gamma/2} u_n \cdot \Lambda^{\gamma/2} \varphi_{1,n} dx + d_{12} \int_{\Omega} \Lambda^{\gamma/2} v_n \cdot \Lambda^{\gamma/2} \varphi_{1,n} dx \\ &= \int_{\Omega} F(u_n^+, v_n^+) \varphi_{1,n} dx, \end{aligned} \quad (5.3)$$

$$\int_{\Omega} \partial_s v_n \varphi_{2,n} dx + d_{22} \int_{\Omega} \Lambda^{\gamma/2} v_n \cdot \Lambda^{\gamma/2} \varphi_{2,n} dx = \int_{\Omega} G(u_n^+, v_n^+) \varphi_{2,n} dx. \quad (5.4)$$

Next, we substitute $\varphi_{1,n} = u_n$ and $\varphi_{2,n} = v_n$ in (5.3) and (5.4), respectively. Then integrating over $(0, t)$ and using Young and Gronwall inequalities, we get for $t \in [0, t')$

$$\begin{aligned} \|v_n\|_{L^\infty(0,t; L^2(\Omega))} &\leq C, \\ \int_0^t \int_{\Omega} \left| \Lambda^{\gamma/2} u_n \right|^2 dx ds + \int_0^t \int_{\Omega} \left| \Lambda^{\gamma/2} v_n \right|^2 dx ds &\leq C, \end{aligned}$$

for some constant $C > 0$ not depending on n .

The next step is to show that the local solution constructed above can be actually extended to the whole time interval $[0, T)$ (independent of n). We stress that this can be done as in [Bendahmane and Karlsen \(2006\)](#), so we omit the details.

Now, if we choose $\varphi_{1,n} = -u_n^-$, $\varphi_{2,n} = -v_n^-$ in (5.3) and (5.4), respectively, then after integration over $(0, t)$ with $0 < t \leq T$, we readily obtain the non-negativity of the solution (u_n, v_n) .

With the help of a compactness tool inspired by Kruzhkov lemma ([Kruzhkov 1969](#)), we justify that the solutions (u_n, v_n) is relatively compact in $L^1(Q_T)$. From this we can extract subsequences, which we do not relabel and we can assume that there exist limit functions u, v such that as $n \rightarrow \infty$

$$\begin{cases} u_n \rightarrow u, v_n \rightarrow v \text{ strongly in } L^1(Q_T) \text{ and a.e. in } Q_T, \\ u_n \rightharpoonup u, v_n \rightharpoonup v \text{ weakly in } L^2(0, T; \tilde{H}^\gamma(\Omega)), \\ F(u_n, v_n) \rightarrow F(u, v), G(u_n, v_n) \rightarrow G(u, v) \text{ in } L^1(Q_T) \text{ a.e. in } Q_T. \end{cases} \quad (5.5)$$

Keeping in mind (5.5) and using the following weak formulation:

$$\begin{aligned} & - \int \int_{Q_T} u_n \partial_t \varphi_1 dx dt + d_{11} \iint_{\Omega} \Lambda^{\gamma/2} u_n \cdot \Lambda^{\gamma/2} \varphi_{1,n} dx dt \\ &+ d_{12} \iint_{\Omega} \Lambda^{\gamma/2} v_n \cdot \Lambda^{\gamma/2} \varphi_{1,n} dx dt \end{aligned}$$

$$\begin{aligned}
&= - \int_{\Omega} u_0(x) \varphi_1(0, x) dx + \iint_{Q_T} F(u_n, v_n) \varphi_1 dx dt, \\
&- \int \int_{Q_T} v_n \partial_t \varphi_2 dx dt + d_{22} \iint_{\Omega} \Lambda^{\gamma/2} v_n \cdot \Lambda^{\gamma/2} \varphi_{2,n} dx dt \\
&= - \int_{\Omega} u_0(x) \varphi_1(0, x) dx + \iint_{Q_T} G(u_n, v_n) \varphi_2 dx dt,
\end{aligned}$$

for all $\varphi_1, \varphi_2 \in \mathcal{D}([0, T) \times \Omega)$, we can let $n \rightarrow \infty$ and obtain a weak solution.

References

- Andreianov B, Bendahmane M, Ruiz-Baier R (2011) Analysis of a finite volume method for a cross-diffusion model in population dynamics. *Math Models Methods Appl Sci* 21:307–344
- Baeumer B, Kovács M, Meerschaert MM (2007) Fractional reproduction-dispersal equations and heavy tail dispersal kernels. *Bull Math Biol* 69(7):2281–2297
- Bendahmane M (2010) Weak and classical solutions to predator-prey system with cross-diffusion. *Nonlinear Anal* 73(8):2489–2503
- Bendahmane M, Bürger R, Ruiz-Baier R, Schneider K (2009) Adaptive multiresolution schemes with local time stepping for two-dimensional degenerate reaction-diffusion systems. *Appl Numer Math* 59:1668–1692
- Bendahmane M, Karlsen KH (2006) Analysis of a class of degenerate reaction-diffusion systems and the bidomain model of cardiac tissue. *Netw Heterog Media* 1(1):185–218
- Berres S, Ruiz-Baier R (2011) A fully adaptive numerical approximation for a two-dimensional epidemic model with nonlinear cross-diffusion. *Nonlinear Anal Real World Appl* 12:2888–2903
- Bouchard JP, Georges A (1990) Anomalous diffusion in disordered media: statistical mechanics, model and physical application. *Phys Rep* 195:127–293
- Brockmann D (2009) Human mobility and spatial disease dynamics. In: Schuster HG (ed) *Rev Nonlinear Dyn Complex*. Wiley-VCH, New York, pp 1–24
- Brockmann D, Hufnagel L, Geisel T (2006) The scaling laws of human travel. *Nature* 439:462–465
- Buchanan M (2008) Ecological modelling: the mathematical mirror to animal nature. *Nature* 453:714–716
- Concezzi M, Spigler R (2012) Numerical solution of two-dimensional fractional diffusion equations by a high-order ADI method. *Commun Appl Ind Math* 3(2):e-421
- De Jager M, Weissing FJ, Herman PM, Nolet BA, Van de Koppel J (2011) Lévy walks evolve through interaction between movement and environmental complexity. *Science* 332(6037):1551–1553
- Eymard R, Gallouët T, Herbin R (2000) Finite volume methods. In: Ciarlet PG, Lions JL (eds) *Handbook of numerical analysis*, vol VII. North-Holland, Amsterdam, pp 713–1020
- Gafiychuk VV, Datsko BY (2006) Pattern formation in a fractional reaction-diffusion system. *Phys A* 365:300–306
- Gambino G, Lombardo MC, Sammartino M, Sciacca V (2013) Turing pattern formation in the Brusselator system with nonlinear diffusion. *Phys Rev E* 88:042925
- Golovin AA, Matkowsky BJ, Volpert VA (2008) Turing pattern formation in the Brusselator model with super-diffusion. *SIAM J Appl Math* 69:251–272
- Hanert E, Schumacher E, Deleersnijder E (2011) Front dynamics in fractional-order epidemic models. *J Theor Biol* 279(1):9–16
- Henry BI, Langlands TAM, Wearne SL (2005) Turing pattern formation in fractional activator-inhibitor systems. *Phys Rev E* 72:026101
- Henry BI, Wearne SL (2002) Existence of Turing instabilities in a two-species fractional reaction-diffusion system. *SIAM J Appl Math* 62:870–887
- Horstmann D (2007) Remarks on some Lotka-Volterra type cross-diffusion models. *Nonlinear Anal Real World Appl* 8:90–117
- Hufnagel L, Brockmann D, Geisel T (2004) Forecast and control of epidemics in a globalized world. *Proc Natl Acad Sci USA* 101:15124–15129
- Jüngel A (2010) Diffusive and nondiffusive population models. *Mathematical Modeling of Collective Behavior in Socio-Economic and Life Sciences*. Birkhäuser, Boston

- Kruzhkov SN (1969) Results on the nature of the continuity of solutions of parabolic equations and some of their applications. *Mat Zametki* 6(1):97–108 (English tr. in. *Math. Notes* 6(1):517–523)
- Langlands TAM, Henry BI, Wearne SL (2007) Turing pattern formation with fractional diffusion and fractional reactions. *J Phys Condens Matter* 19:065115
- Li BW, Wang J (2003) Anomalous heat conduction and anomalous diffusion in one-dimensional systems. *Phys Rev Lett* 91:044301
- Lou Y, Ni WM (1996) Diffusion, self-diffusion and cross-diffusion. *J Diff Eqs* 131:79–131
- Lou Y, Nagy Laki T, Ni WM (2001) On diffusion-induced blowups in a mutualistic model. *Nonlinear Anal Theory Meth Appl* 45:329–342
- Metzler R, Klafter J (2000) The random walk's guide to anomalous diffusion: A fractional dynamics approach. *Phys Rep* 339:1–77
- Meerschaert MM, Tadjeran C (2006) Finite difference approximations for two-sided space-fractional partial differential equations. *Appl Numer Math* 5(6):80–90
- Metzler R, Klafter J (2000) The random walk's guide to anomalous diffusion: a fractional dynamics approach. *Phys Rep* 339:1–77
- Metzler R, Klafter J (2004) The restaurant at the end of the random walk: recent developments in the description of anomalous transport by fractional dynamics. *J Phys A* 37:R161
- Nec Y, Nepomnyashchy AA, Golovin AA (2008) Oscillatory instability in super-diffusive reaction-diffusion systems: fractional amplitude and phase diffusion equations. *Europhys Lett* 82:58003
- Nec Y, Nepomnyashchy AA (2007) Turing instability in sub-diffusive reaction-diffusion systems. *J Phys A* 40:14687–14702
- Nec Y, Nepomnyashchy AA (2008) Turing instability of anomalous reaction-anomalous diffusion systems. *Eur J Appl Math* 19:329–349
- Okubo A, Levin S (2002) Diffusion and Ecological Problems: Modern Perspectives. Springer, New York
- Pearson JE (1993) Complex patterns in a simple system. *Science* 261:189–192
- Ramos-Fernandez G, Mateos JL, Miramontes O, Cocho G, Larralde H, Ayala-Orozco B (2004) Lévy walk patterns in the foraging movements of spider monkeys (*ateles geoffroyi*). *Behav Ecol Sociobiol* 55(3):223–230
- Schmitt FG, Seuront L (2001) Multifractal random walk in copepod behavior. *Phys A* 301:375–396
- Sims DW, Southall EJ, Humphries NE, Hays GC, Bradshaw CJ, Pitchford JW, James A, Ahmed MZ, Brierley AS, Hindell MA et al (2008) Scaling laws of marine predator search behaviour. *Nature* 451(7182):1098–1102
- Sokolov IM, Klafter J, Blumen A (2002) Fractional kinetics. *Phys Today* 55:48–54
- Toner J, Tu Y, Ramaswamy S (2005) Hydrodynamics and phases of flocks. *Ann Phys* 318:170–244
- Viswanathan GM, Afanasyev V, Buldyrev SV, Murphy EJ, Prince PA, Stanley HE (1996) Lévy flight search patterns of wandering albatrosses. *Nature* 381:413–415
- Weiss M (2003) Stabilizing Turing patterns with subdiffusion in systems with low particle numbers. *Phys Rev E* 68:036213
- Yadav A, Horsthemke W (2006) Kinetic equations for reaction-subdiffusion systems: derivation and stability analysis. *Phys Rev E* 74:066118
- Yadav A, Milu SM, Horsthemke W (2008) Turing instability in reaction-subdiffusion systems. *Phys Rev E* 78:026116
- Yang Q, Liu F, Turner I (2010) Numerical methods for fractional partial differential equations with Riesz space fractional derivatives. *Appl Numer Model* 34:200–218